Characterization of Biological Thin Films at the Solid-Liquid Interface by X-Ray Reflectivity

C. E. Miller,[1] J. Majewski,[2] T. Gog,[3] and T. L. Kuhl[4]

[1]*Biophysics Graduate Group, University of California, Davis, California 95616, USA*
[2]*Manuel Lujan Neutron Scattering Center, Los Alamos National Laboratory, Los Alamos, New Mexico 87545, USA*
[3]*Advanced Photon Source, Argonne National Laboratory, Argonne, Illinois 60439, USA*
[4]*Department of Chemical Engineering and Material Science, University of California, Davis, California 95616, USA*

(Received 23 July 2004; published 16 June 2005)

We demonstrate that 18 keV x rays can be used to study organic thin films at the solid-liquid interface by x-ray reflectivity. We establish that this is a powerful technique for investigating biological systems in a previously inaccessible manner. Our measurements enabled the density distribution of single phospholipid bilayer membranes in bulk water to be measured with unprecedented precision. Previously, characterization of biomimetic structures normal to a ''buried'' interface was a domain of neutron reflectivity.

DOI: 10.1103/PhysRevLett.94.238104 PACS numbers: 87.16.Dg, 82.45.Mp

Similar to neutron reflectivity (NR), specular x-ray reflectivity (XR) using synchrotron radiation is a powerful method for determining the structure of thin films. Because the interaction strength of neutrons with matter is typically an order of magnitude less than that for x rays, neutrons have been considered the ideal particle for performing reflectivity measurements on samples where the beam must pass through several centimeters of material to reach a buried interface. Conversely, the usual incident energy in XR is $\sim$10 keV, making it very surface sensitive but lacking penetration power. As a result, XR studies have been generally limited to thin films at the solid-air or liquid-air interface. Recently, there have been several reports on x-ray investigation of buried interfaces using high-energy synchrotron radiation [1–10]. These include x-ray reflectivity and x-ray standing wave studies of thin layers at the solid-liquid interface. However, these investigations lack biological relevance.

Here, we report novel results characterizing single phospholipid bilayer membranes at the solid-water interface using 18 keV photons. Because of the great complexity of cellular membranes, their study demands simplification without losing the structure, properties, and function of the bilayer. This can be accomplished by using model membranes that are designed to mimic the structure and function of cellular membranes under physiological conditions [11]. For example, investigation of lipid membranes at the solid-liquid interface enables the use of high-resolution surface science techniques including atomic force microscopy, ellipsometry, surface plasmon resonance, and neutron reflectivity. In particular, NR, where the neutron beam penetrates through the solid support, has been used to study the structure of hybrid bilayer membranes [12,13] and polymer cushioned bilayers [14,15]. Krueger's review provides an excellent summary of recent work in the field [11]. Utilizing the advantages of XR (described below) in tandem with the benefits of NR (i.e., contrast variation and little beam damage) will be extremely influential in the study of soft condensed matter systems. Fragneto and coworkers have recently discussed the use of these complementary techniques [16,17].

In this work, we demonstrate the use of high-energy photons to characterize the structure of a 1,2-Dioleoyl-*sn*-Glycero-3-Phosphocholine (DOPC) fluid-phase bilayer and a 1:9 1,2-Dilauryl-*sn*-Glycero-3-Phosphocholine (DLPC):1,2-Distearyl-*sn*-Glycero-3-Phosphocholine (DSPC) predominantly gel-phase bilayer at the solid-liquid interface in bulk water. This is the first such work dealing with biology-related membranes and x-ray reflectometry at the solid-water interface.

Third generation synchrotron x-ray source intensities are typically 10 orders of magnitude more intense than current neutron sources. Because of low incident fluxes, neutron reflectivity experiments of thin layers at the solid-liquid interface typically utilize a probed substrate area of at least 500 mm^2 with a length of the sample along the beam of $\sim$50 mm to maximize the signal of the reflected beam. Still, reflectivity measurements out to momentum transfer vector Q_z values of $\sim$0.2–0.3 $Å^{-1}$ require 3–4 h of acquisition time [13,15,18,19]. This Q_z range limits the real-space resolution [20]. Sample lengths of this magnitude are not tenable for x-ray reflectivity utilizing wavelengths of $\sim$1.5 Å, due to beam attenuation by the liquid layer or solid support. To overcome this, we decreased the path length of the x rays through the liquid (water) and increased their energy. Specifically, we used single crystal quartz substrates with dimensions 10×50 mm^2 as the solid support. The substrate was placed in a water filled, stainless steel cell (with Kapton windows) [Fig. 1(a)] and oriented so that the 10 mm dimension was along the x-ray beam. To increase the transmission, we used high-energy x rays (18 keV, $\lambda \approx 0.65$ Å). These much more energetic photons penetrate through the thick water layer with a transmission of approximately 40% [21]. For comparison, the transmission is less than 1% at 10 keV.

At the CMC-CAT beam line at the APS synchrotron source, we measured the reflectivity from substrate-supported bilayers out to a momentum transfer of

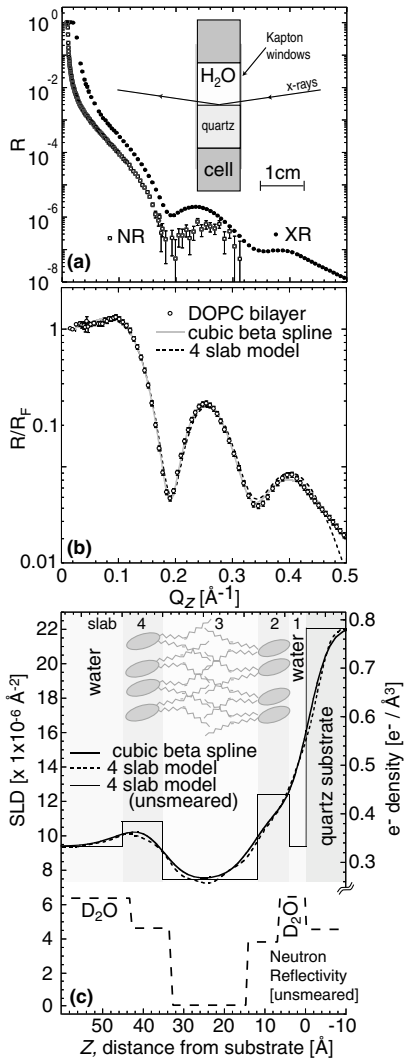

FIG. 1. (a) Comparison of the data from neutron reflectivity (NR) and x-ray reflectivity (XR) demonstrating the increased dynamic range of x rays. Inset: schematic cross section of the sample cell. (b) Measured x-ray reflectivity plotted as R/R_{Fresnel} versus Q_z, where R_{Fresnel} is the reflectivity of an infinitely sharp, steplike interface. This removes the sharp drop of reflectivity due to the R_{Fresnel} dependence and enhances visibility of the interference fringes [35]. Error bars for the reflectivity data represent statistical errors in these measurements. (c) Scattering length density (SLD) profiles of a DOPC fluid bilayer at the solid-liquid interface at 20 °C. The head groups and hydrocarbon tail region of the bilayer can clearly be distinguished along with a 4 Å water cushion layer between the bilayer and the substrate. The 4-slab model (dashed line) and cubic beta spline calculation (solid line) are very close in agreement. The lower, dashed line shows a comparison of the unsmeared (zero interfacial roughness) SLD profiles measured by NR. The lengths of each region are consistent between techniques. For simplicity, we have not discussed more complex methods of refining the membrane structure, which can be based on quasimolecular composition-space refinement [34]. Note that the SLD of x rays is defined by multiplying the electron density $[e^-/\text{Å}^3]$ of the material by 2.82×10^{-5} Å. The electron density of water is $0.334e^-/\text{Å}^3$.

0.5 Å^{-1} covering 8 orders in the dynamic range of intensity. This was done without the extraordinary efforts and specific circumstances needed for acquiring higher-resolution NR data [22]. We were thus able to probe electron density differences on a length scale almost 2 times smaller (e.g., $Q_z = 0.5$ vs 0.3 Å^{-1}) [20]. Two bilayer compositions were investigated; fluid DOPC and 1:9 DLPC:DSPC gel-phase membranes formed by vesicle fusion [23] on single crystal quartz substrates. X-ray reflectivity scans were completed in approximately 30 min. Further refinements, such as an increased vertical slit size at higher angles, should allow reflectivity data collection out to Q_z values of $\sim$1.0 Å^{-1} with a commiserate increase in resolution.

At low angles, the beam footprint was larger than the sample length. Therefore, the intensity of the incident beam intercepted by the sample was not constant over the entire Q_z range. To account for this difference, the data [24] were renormalized by dividing the specular reflectivity by $\sin\theta$ up to the angle where the size of the beam footprint equaled the sample length along the beam.

The results from a fluid DOPC bilayer deposited by vesicle fusion are shown in Fig. 1. A simple 4-slab (outer head group, hydrocarbon tails, inner head group, and water cushion) XR model, based on the Parratt algorithm [25], fits the data with a reduced χ^2 value of 5.3 with only small deviation in the scattering length density (SLD) profile from the free form, model independent, cubic beta spline approach [26]. The thickness of the hydrocarbon region was 23.2 Å. This value is in excellent agreement with the theoretical calculation of 24 Å for a fluid-phase bilayer (80 Å^2/lipid) with 18 carbons per lipid tail [27,28]. From the fitting model, it can also be seen that the inner head group region has a higher scattering length density than the outer head group region, indicative of lower water content. In addition, the thickness of the outer head group region was 10 Å with a 6 Å roughness, while the inner head group thickness was 8 Å with a 3.8 Å roughness. This finding is consistent with a reduction in motion of the inner leaflet lipids due to interactions with the solid support and a concomitant reduction of fluctuations [29,30]. The bilayer was separated from the quartz substrate by a thin 4 Å water layer. For comparison, we also measured this sample using neutron reflectivity. In both cases, the length scales of the four slabs were consistent between NR and XR. These findings for the DOPC bilayer are also in agreement with work published by Johnson *et al.* of neutron reflectivity done on a DMPC lipid bilayer at the quartz-water interface [31].

The reflectivity profile from a 1:9 DLPC:DSPC bilayer deposited by vesicle fusion is shown in Fig. 2. At room temperature, these lipids phase separate due to their large difference in tail length (18 carbons for DSPC and 12 carbons for DLPC). The phase transition temperature (T_{melt}) of DLPC is -2 °C, and T_{melt} for DSPC is 55 °C [28]. There

are several possible arrangements of the two lipid components. For example, previous studies using atomic force microscopy (AFM), determined that DSPC and DLPC phases separated into coupled domains with an 18 Å height difference [32].

Our modeling took into account several membrane structures including phase separation, preferential leaflet segregation, and leaflet coupling with either inner leaflet head groups aligned or tail groups aligned between leaflets. Two specific models are depicted schematically in Fig. 2(b). Although the lipid components in the mixture are expected to phase separate, the composite membrane must be relatively flat (low variation in film thickness) due to coupling with the substrate and the absence of significant off-specular scattering in the reflectivity data. Overall, we found that the best fit to the data (lowest χ^2) required 5 slabs (upper schematic). The best fit was consistent with (1) a water cushion, (2) a pure DSPC head group region, (3) a tail region consisting of an inner DSPC leaflet and an outer mixed leaflet of DSPC and DLPC tails, (4) a mixed DSPC tail–DLPC head group, and (5) an outer DSPC head group–water region. In all cases, 5-slab models drove the hydrocarbon tail region (slab 3) to a thickness of 26 ± 2 Å, which is significantly larger than the expected thickness of two fully stretched C_{12} chains for DLPC (e.g., 19 Å), a strong indication of preferential leaflet segregation. The inner leaflet head group SLD of $14.0 \times 10^{-6} \pm 0.3 \times 10^{-6}$ Å^{-2} also matches well to the expected SLD for gel-phase DSPC. Because the interaction of the membrane with the substrate suppresses fluctuations [29,30], it is entropically less costly for the gel-phase DSPC to preferentially segregate to the inner leaflet compared to fluid-phase DLPC. We hypothesize that this is the driving force for the observed leaflet segregation. However, because the difference in SLD between gel-phase and fluid-phase tails is small, we cannot unequivocally rule out the inverse of this model-preferential segregation of DLPC to the inner leaflet. Again, a 5–6 Å water ''cushion'' layer between the bilayer and the substrate was required in good agreement with our results for DOPC. We also tested various 6-slab models [33], including a symmetric profile (about the plane where the alkyl tails meet) that contained four head group regions (two for the DLPC head group and two for the DSPC head group) as shown in Fig. 2(b) (bottom schematic). This more complicated model resulted in a larger χ^2 value (8.7 vs 5.1), demonstrating that XR provides adequate resolution to distinguish between these various models.

In conclusion, x-ray reflectivity has the resolution increase needed to distinguish between real-space lipid membrane structures. In all our studies extreme care was used to minimize damage caused by the high flux x-ray beam by frequently moving the sample perpendicular to the beam during specular scans. As can be seen from our results, there is high correspondence of the SLD profiles between the cubic spline and slab model fits. The differences at high Q_z regions between the model fits and the data may be due to the following factors: errors in renormalization procedure, simplicity of the slab models, a need for more sophisticated fitting procedures to describe the SLD of the membranes [34], and possible beam damage. A

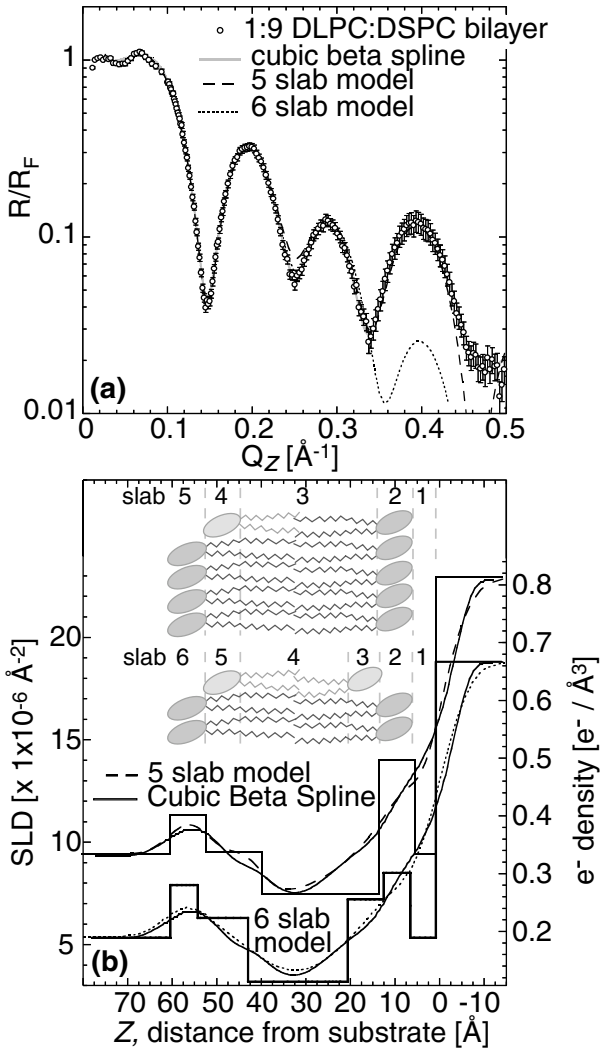

FIG. 2. (a) Measured x-ray reflectivity profile and (b) scattering length density (SLD) for a 1:9 DLPC:DSPC bilayer. In this system, there is a large difference in hydrocarbon tail length between the two lipids present. As a result, the lipid layers arrange to minimize the amount of hydrophobic tail exposed to water. Reproducing this effect in a box model required 5 slabs ($\chi^2 = 5.1$) in a nonsymmetric configuration with the inner leaflet head groups aligned at the quartz interface. This arrangement of lipids is shown in the upper schematic. The SLD profile from a cubic beta spline calculation is shown for comparison. A number of structural models were examined. The result from a 6-slab model ($\chi^2 = 8.7$, shifted down by 4×10^{-6} Å^{-2}) in a symmetrical configuration (tail groups aligned) is shown below (lower schematic). Error bars for the reflectivity data represent statistical errors in these measurements.

natural extension of these studies is to probe in-plane membrane or bilayer structure using grazing incidence diffraction (work in progress), a technique inaccessible to neutrons and previously limited to lipid monolayers at the liquid-air interface.

The ability to do x-ray reflectivity measurements at the solid-solution interface enabled the density distribution of lipid membranes to be measured in a previously inaccessible manner. The increased resolution allowed subtle features in membrane structure and leaflet segregation to be revealed. The advantages of using x rays over neutrons are higher flux (increased resolution), smaller sample sizes, faster measurements using more accessible synchrotron sources, no requirements of using expensive deuterated molecules, and the opportunity of exploiting grazing incidence diffraction. These successful measurements of bilayers at the solid-liquid interface will lead to a new arsenal of x-ray experiments on other biological systems and thin films.

This work was supported by University of California directed research and development funds, Los Alamos National Laboratory under DOE Contract No. W7405-ENG-36, and by the DOE Office of Basic Energy Science. The work at the CMC Beamline is supported in part by the Office of Basic Energy Sciences of the U.S. Department of Energy and by the National Science Foundation Division of Materials Research. The use of the Advanced Photon Source is supported by the Office of Basic Energy Sciences of the U.S. Department of Energy under Contract No. W-31-109-Eng-38.

[1] S. J. Roser, R. Felici, and A. Eaglesham, Langmuir **10**, 3853 (1994).
[2] M. L. Schlossman, Curr. Opin. Colloid Interface Sci. **7**, 235 (2002).
[3] A. G. Richter *et al.*, Phys. Rev. E **61**, 607 (2000).
[4] F. Rieutord *et al.*, Phys. Rev. B **63**, 125408 (2001).
[5] H. Reichert *et al.*, Physica (Amsterdam) **336B**, 46 (2003).
[6] S. Engemann *et al.*, Phys. Rev. Lett. **92**, 205701 (2004).
[7] G. Scherb, A. Kazimirov, and J. Zegenhagen, Rev. Sci. Instrum. **69**, 512 (1998).
[8] J. Wang *et al.*, J. Phys. Chem. **98**, 10 957 (1994).
[9] J. Wang *et al.*, Langmuir **17**, 3671 (2001).
[10] R. T. Zhang, R. Itri, and M. Caffrey, Biophys. J. **74**, 1924 (1998).
[11] S. Krueger, Curr. Opin. Colloid Interface Sci. **6**, 111 (2001).
[12] B. W. Koenig *et al.*, Langmuir **12**, 1343 (1996).
[13] C. F. Majkrzak *et al.*, Biophys. J. **79**, 3330 (2000).
[14] J. Y. Wong *et al.*, Biophys. J. **77**, 1445 (1999).
[15] J. Majewski *et al.*, Biophys. J. **75**, 2363 (1998).
[16] G. Fragneto *et al.*, in Proceedings of the 20th General Conference of the Condensed Matter Division of the European Physics Society, Prague, 2004 (unpublished).
[17] G. Fragneto *et al.*, Physica (Amsterdam) **276B**, 501 (2000).
[18] A. V. Hughes *et al.*, Langmuir **18**, 8161 (2002).
[19] S. Krueger *et al.*, Langmuir **11**, 3218 (1995).
[20] U. A. Perez-Salas *et al.*, Langmuir **19**, 7688 (2003).
[21] B. L. Henke, E. M. Gullikson, and J. C. Davis, At. Data Nucl. Data Tables **55**, 349 (1993).
[22] S. Krueger *et al.*, Langmuir **17**, 511 (2001).
[23] A. E. McKiernan *et al.*, Biophys. J. **73**, 1987 (1997).
[24] Background was measured off the specular beam (on both sides of the specular reflection) for all points, and rocking curve scans were performed at several incidence angles to check alignment.
[25] L. G. Parratt, Phys. Rev. **95**, 359 (1954).
[26] J. S. Pedersen and I. W. Hamley, Physica (Amsterdam) **198B**, 16 (1994).
[27] J. Marra and J. Israelachvili, Biochemistry **24**, 4608 (1985).
[28] D. Marsh, *CRC Handbook of Lipid Bilayers* (CRC Press, Inc., Boca Raton, FL, 1990).
[29] T. L. Kuhl *et al.*, Biophys. J. **75**, 2352 (1998).
[30] M. Hetzer *et al.*, Langmuir **14**, 982 (1998).
[31] S. J. Johnson *et al.*, Biophys. J. **59**, 289 (1991).
[32] T. V. Ratto and M. L. Longo, Biophys. J. **83**, 3380 (2002).
[33] Note that other 6-slab models consistently degenerated into 5-slab models similar to the 5-slab model reported in Fig. 2.
[34] M. Schalke *et al.*, Biochim. Biophys. Acta, Biomembr. **1464**, 113 (2000).
[35] J. Als Nielsen *et al.*, Phys. Rep., Rev. Sect. Phys. Lett. **246**, 252 (1994).